

THEORETICAL STUDIES ON THE NEW HIGH-NITROGEN EXPLOSIVES N14 AND N18

Jifeng Chen^a, Yi Yu^b, Yuchuan Li^{a,*} and Siping Pang^{a,#}^aSchool of Materials Science & Engineering, Beijing Institute of Technology, 100081 Beijing – PR, China^bResearch Institute of Aerospace Special Materials and Processing Technology, 100074 Beijing – PR, China

Recebido em 10/02/2019; aceito em 18/07/2019; publicado na web em 30/08/2019

The power of a compound is enhanced by the direct connection of nitrogen atoms, and its stability can be improved through conjugated structure. So novel high energy density materials N14 (1,6-dihydro-1,2,3,3a,4,5,5a,6,7,8,8a,9,10,10a-tetradecazapyrene) and N18 (1,2,2a,3,4,4a,5,6,6a,7,8,8a,9,10,10a,11,12a-octadecazacoronene) were designed, and their structures, detonation performance, and stabilities were calculated employing density functional theory (DFT). The detonation performance includes detonation pressure (P), detonation velocity (D), and heat of detonation (Q). Furthermore, the stability involves frontier molecular orbitals and impact sensitivity. Calculations reveal that they have an excellent power, detonation performance of N14 ($P = 43.6$ GPa, $D = 10040$ m s⁻¹, $Q = 2214$ cal g⁻¹) and N18 ($P = 37.4$ GPa, $D = 9400$ m s⁻¹, $Q = 2114$ cal g⁻¹) are comparable to CL-20. Besides, their impact sensitivities are slightly better than CL-20, therefore they are promising candidates in energetic materials.

Keywords: N14; N18; density functional theory (DFT); high energy; high-nitrogen.

INTRODUCTION

High energy density materials (HEDMs), which possess not only perfect detonation performance, but also good thermal stability and low sensitivity, have attracted considerable interest for some potential applications in propellants, explosives, and pyrotechnic agents in recent years.¹⁻³ In order to meet the main requirements in safety and power, much effort has been made by a large number of research groups.⁴⁻⁷ However, in most cases, it is very difficult to concentrate both desired properties into one substance. Traditional energetic materials (HMX, RDX, CL20, etc.) are developing toward a bottleneck stage.

Polynitrogen materials have received much more attention on their high energy content due to the deviation of bond energy of the N₂ triple bond and N-N single bonds or double bonds.⁸ However, most of them are unstable. Since 1999, a series of N₅⁺-containing salts have been investigated and the most stable N₅⁺-containing salt N₅⁺SbF₆⁻ is only stable at about 60 °C.⁷ In 2004, polymeric nitrogen with a cubic gauche structure was produced by Eremets.⁹ Its power is five times greater than that of the most powerfully energetic materials, whereas it disappears at ambient pressure. In 2017, two significant breakthroughs in the bulk synthesis and characterization of the pentazolite anion cyclo-N₅⁻ salts were achieved by Lu and Hu, respectively.^{5,10} Recently, the most stable cyclo-N₅⁻ salts, Na₂₄N₆₀ and Na₂₀N₆₀, occur only below 148 °C.¹¹ Additionally, some other all-nitrogen materials cannot exist under room temperature for a long period.^{8,12}

New high energy density materials are considered under the circumstances. Two novel covalent compounds, N14 and N18, are designed in this paper with the characteristics of great power and high safety, whose chemical structures are shown in Figure 1. There are 14 nitrogen atoms closely linked in N14, and 18 nitrogen atoms in N18. In these structures, several nitrogen atoms connected directly can enhance energy. However, in most cases, high nitrogen content and stability tend to be mutually exclusive.⁴ Thereby olefin and benzene ring are expected to form a large π bond with nitrogen atoms to improve its stability, though the large conjugated bonds do not

appear. The C₁₂N₁₂ structure, being similar to N18, was reported, and Mondal¹³ indicates that is slightly aromatic in nature, but Tursungul¹⁴ does not agree with him.

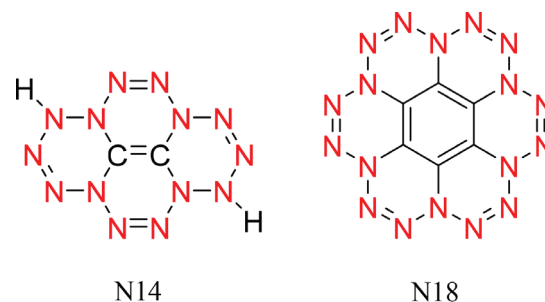


Figure 1. Chemical structure of the title compounds

Theoretical studies of N14 and N18 make it not only possible to provide a forecast of the properties of candidate compounds, but it is also possible to compare them. The theoretical density (ρ), the heat of formation (HOF), and the detonation performance is emphasized to explain their high energy. At the same time, the molecular geometries' structures, impact sensitivity $h_{50\%}$ and electrostatic potential (ESP) is present to illustrate their relatively stable. Besides, the frontier molecular orbitals and possible synthetic routes are also expounded. These results can be used for comparison with the properties of some familiar explosives and polynitrogen materials, providing theoretical support for the molecular design of novel high energy density compounds.

COMPUTATIONAL DETAILS

Computations were performed with the Gaussian 09 package at the B3LYP level¹⁵ method with the 6-311++G (d, p) basis set. The B3LYP method is a common and effective way to evaluate energetic compounds, which was mentioned in previous papers.¹⁶⁻¹⁹ The molecular geometries and electronic structures were obtained with the density functional theory (DFT) method. The geometric parameters of these two structures were allowed to be optimized, and no constraints were imposed on the molecular structures during the

*e-mail: liyuchuan@bit.edu.cn

#alternative e-mail: pangsp@bit.edu.cn

optimization process. Structures were identified to be local minima without imaginary frequencies.

The geometric structure refers to the bond length and bond angle in this paper. Bond length is one important parameter for a molecule. Commonly, the bond length is closely related with the bond stability: the longer the bond length is, the less stable the bond is.²⁰ Bond angle is another important parameter for a molecule and 108° is an excellent value.¹⁷

Molecular electrostatic potentials (ESP) are used to describe the interaction of static electricity in molecules, and to predict chemical reactivity sites. The results of ESP can be viewed and analyzed by the visual molecular dynamics (VMD), which is a molecular modelling and visualization computer program.²¹ With the help of the VMD program, the very nice color-filled molecular surface maps with surface extrema can be plotted based on the output of the Multiwfn program.²² In the maps, Figures 7 and 8, the green and orange spheres correspond to significant minima and maxima ESP surfaces, respectively. These spheres are labeled by dark blue and brown-red texts with the unit kcal mol⁻¹. At the same time, the global minima and maxima on the surface are labeled by larger and italic font.

The isodesmic reactions were used to predict the heat of formation (HOF) of compounds, and isodesmic reactions of N14 and N18 are shown in Figures 2 and 3. The enthalpy of reaction ($\Delta_r H_{298}$) at 298 K can be calculated according to Equation (1) in the isodesmic reaction. The $\Delta_f H_P$ and $\Delta_f H_R$ of the following equation are the HOFs of products and the reactants, respectively. Similarly, ΔE_0 , ΔE_{ZPE} , and ΔH_T are the differences between products and reactants. Furthermore, the E_0 is the total energy at 0 K and the ΔH_T is the thermal correction from 0 K to 298 K. The E_{ZPE} is zero-point energy, which means the difference between the lowest possible energy that a quantum mechanical system may have, and the classical minimum energy of the system.

According to Equation (1), the heat of formation of the gaseous N14 and N18 $\Delta_f H(g)$ can be calculated, while the heat of formation in the condensed phase $\Delta_f H(c)$ is determined by Equation (2). In order to estimate ΔH_{sub} , the electrostatic potential method²³ can be used, as shown in Equation (3). In the equation (3) and (4), A_s is molecular surface area. And σ_{tot}^2 is total variance on the molecular surface, which is the sum of positive and negative parts and reflects the variability of molecular electrostatic potentials. The v is electrostatic balance parameter, and the value of $v\sigma_{tot}^2$ indicates that a molecule has relatively strong tendencies to interact with others of its own kind electrostatically. Finally, these parameters can be calculated by Multiwfn software.²²

$$\begin{aligned} \Delta_r H_{298} &= \sum \Delta_f H_P - \sum \Delta_f H_R \\ &= \Delta E_0 + \Delta E_{ZPE} + \Delta H_T + \Delta nRT \end{aligned} \quad (1)$$

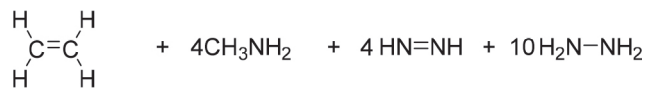
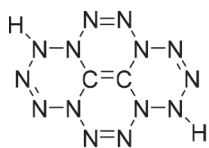


Figure 2. The isodesmic reaction of N14

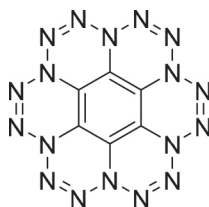


Figure 3. The isodesmic reaction of N18

$$\Delta_f H(c) = \Delta_f H(g) - \Delta H_{sub} \quad (2)$$

$$\Delta H_{sub} = 0.000267(A_s)^2 + 1.650087(v\sigma_{tot}^2)^{0.5} + 2.966078 \quad (3)$$

In the high energy density material, the crystal density (ρ) is an important parameter for predicting performance. Equation (4) proposed by Politzer *et al.*²⁴ was used to calculate the crystal density of compounds where M is the molecular weight and V_m is the molecular volume defined as the inside of a contour of 0.001 au density that was evaluated using Monte Carlo integration. Finally, α , β , and γ here are 0.9183, 0.0028, and 0.0443, respectively.

$$\rho = \alpha \left(\frac{M}{V_m} \right) + \beta (v\sigma_{tot}^2) + \gamma \quad (4)$$

Detonation pressure (P , GPa), detonation velocity (D , km s⁻¹), and heat of detonation (Q , cal g⁻¹) reflecting the explosive performance of energetic materials, were estimated using EXPLO 5 (v6.01).

The frontier molecular orbitals include the lowest unoccupied molecular orbital (LUMO) and the highest occupied molecular orbital (HOMO). Long-range corrected hybrid functionals (ω B97X-D) are considered to be more accurate than global hybrid functionals (B3LYP) when predicting the energy gap,²⁵ while the two methods were used in the paper to illustrate the fact well.

Impact sensitivity is an important index to evaluate explosives, and $h_{50\%}$ is a common value to assess the index. The $h_{50\%}$ is the height where 50% probability of the “drop” results in a reaction of the sample. The shorter the drop height is, the greater the impact sensitivity is. The value is difficult to measure experimentally and strongly depend on morphology, crystal shape and size and impurities. Predicting it with any reliability is even more difficult, but Equation (5) can estimate it approximately. In the equation, α_2 , β_2 , and γ_2 are -0.0064, 241.42, and -3.43, respectively.²⁶

$$h_{50\%} = \alpha_2 \sigma_+^2 + \beta_2 v + \gamma_2 \quad (5)$$

RESULTS AND DISCUSSION

Geometrical structures

The structure of N18 is similar to that of coronene, with periphery nitrogen atoms replacing carbon atoms. Some of periphery nitrogen atoms form double bonds while some form single bonds, and the middle carbon forms the benzene ring. We hope that the nitrogen atoms with single bonds, which carry lone-pair electrons, form larger conjugated systems with the benzene ring and a large number of azo

bonds. However, the output result of the B3LYP method shows that all atoms are not coplanar, so N18 may be not an aromatic compound. The structure output of N18 is shown in Figure 4. Six carbon atoms of the benzene ring form large π bonds in the input structure, but they are linked together with double bonds in the output structure. This is not corrected for the sake of keeping the raw data. More information on standard orientation of every atom was presented in Supporting Information in detail.

In this structure, all carbon atoms are in the same plane and each C-C bond length is 1.3707 Å, which is shorter than that of benzene (1.3945 Å). All of the double-bond nitrogen atoms are also in the same plane and the distance of the N-N double bond (each one is 1.2389 Å) is shorter than that of azobenzene (1.2522 Å). Similarly, six single-bond nitrogen atoms are placed on the same plane while the N-N single bond of the compound (1.4398 Å) is close to that of hydrazine (1.4310 Å) and C-N single bonds of the compound (1.3921 Å) are shorter than C-NO₂ of TATB (1.4366 Å). The bond lengths of the mentioned benzene, azobenzene, hydrazine, and TATB are calculated using the same method with N18. In this structure, C2-C1-C3 = 120.0°, N8-C4-C2 = 119.8°, N7-N8-C4 = 114.2°, N7-N8-N9 = 109.1°, and N8-N9-N10 = 121.7°. Since N18 has a symmetrical structure, other bond angles have the same value and all bond angles are approximately 108°. Therefore, single-bond nitrogen atoms, double-bond nitrogen atoms, and carbon atoms are not on the same plane and form a large conjugated system, but they have special interactions to become a stable structure. Some bond lengths and bond angles of N18 are listed in Table 1.

The structure of N14 is similar to that of pyrene, with periphery nitrogen atoms replacing carbon atoms. Moreover, it possesses two additional hydrogen atoms because nitrogen has three valence bonds. We hope that the nitrogen atoms with single bonds, which carry lone-pair electrons, form a larger conjugated system with the C-C double bond and many azo bonds. Just like N18, the output result

with the B3LYP method shows that all atoms are not coplanar, so N14 may not be an aromatic compound. The structure output of N14 is shown in Figure 5.

In the structure of N14, the C-C double bond has a bond length of 1.3122 Å, which is shorter than that of ethylene (1.3288 Å). The distance between N3-N4 and N9-N10 is 1.2523 Å, while that of N6-N7 and N12-N13 is 1.2324 Å, and they are close to their counterpart of azobenzene. Two C-N bond lengths are 1.3922 and 1.3921 Å, respectively, which are shorter than C-NO₂ of TATB. The N-H bond length is 1.0151 Å, which is close to that of NH₃ (1.0147 Å), calculated with same method and basis set. All N-N single bond lengths of N14 are listed in Table 2. Some of them are shorter than that of hydrazine, and some of them are slightly longer, but close to it. In the structure of N14, some bond angles are also listed in Table 2 and other bond angles have the same value for the symmetrical structure. From the table, it can be seen that all bond angles are close to 108°. As in the situation with N18, not all atoms in N14 are on the same plane and form a large conjugated system, but they have special interactions to become a stable structure. More information on output result of N14 was presented in Supporting Information in detail.

Frontier molecular orbitals

The LUMO (a) and HOMO (b) orbits of N14 and N18 are shown in Figure 6. The positive phase is red and the negative one is green. Either LUMO or HOMO doesn't locate on H atom of N14, and the two orbits locate approximately on all the atoms of N18. Energy gaps of two compounds were calculated with B3LYP and ω B97X-D listed in Table 3. The values of $\Delta E_{\text{LUMO-HOMO}}$ are small, but it only reflects photochemistry stability. Natural bond orbital (NBO) analysis is an essential tool for studying interactions among bonds, and the orbital charges are summarized in the Supporting Information.

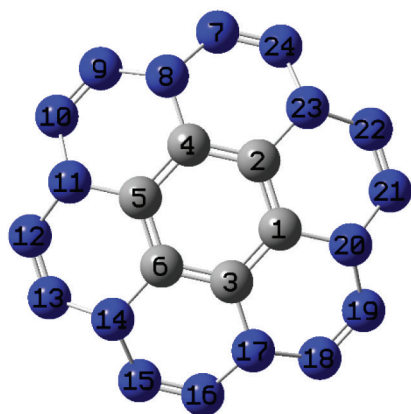


Figure 4. Structure of N18

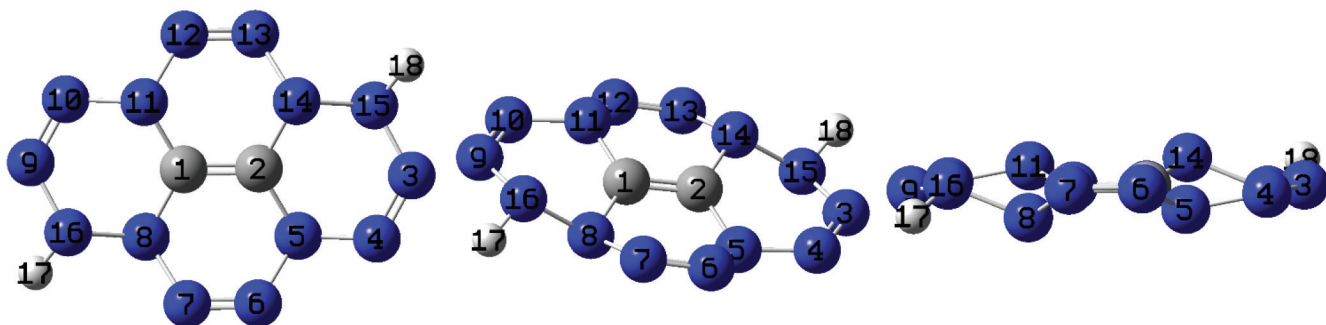


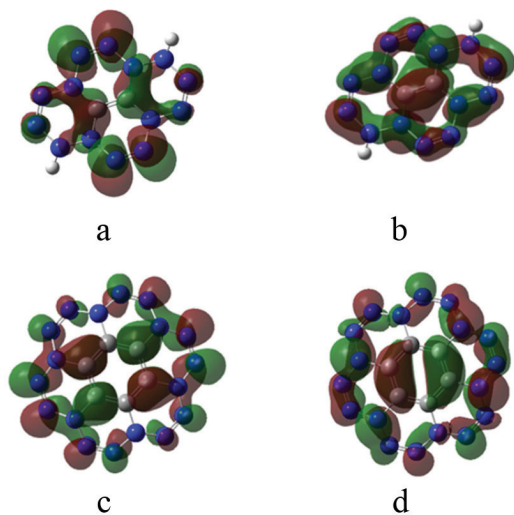
Figure 5. Structure of N14

Table 1. Some bond lengths and bond angles of N18

Bond	Bond length(Å)	Bond	Bond angles (°)
C1-C2	1.3707	C2-C1-C3	120.0
C1-N20	1.3921	N8-C4-C2	119.8
N7-N8	1.4398	N7-N8-C4	114.2
N9-N10	1.2389	N7-N8-N9	109.1
		N8-N9-N10	121.7

Table 2. Some bond lengths and bond angles of N14

Bond	Bond length(Å)	Bond	Bond angles (°)
N4-N5	1.3950	N9-N16-N8	115.3
N9-N16	1.3874	N16-N8-N7	110.4
N5-N6	1.4323	N8-N7-N6	119.0
N8-N16	1.4634	N7-N6-N5	119.4
N7-N8	1.4757	N6-N5-N4	113.0
N10-N11	1.3949	N5-N4-N3	117.8
N3-N15	1.3873	N4-N3-N15	122.2
N11-N12	1.4319	N3-N15-H18	106.4
N14-N15	1.4634		
N13-N14	1.4756		

**Figure 6.** LUMO (a) and HOMO (b) orbitals of N14; and LUMO (c) and HOMO (d) orbitals of N18

Electrostatic potentials

The electrostatic potential map of the molecular surface (a) and the surface areas in each ESP range (b) of N14 are plotted and shown in Figure 7. The surface minima of ESP is distributed near some N atoms due to these atoms with double bonds or lone-pair electron, which are the primary electrophilic sites. The global minima site of

ESP is present near the N3 atom, with the value $-24.03 \text{ kcal mol}^{-1}$. The global maxima site of ESP is $+52.67 \text{ kcal mol}^{-1}$, which is close to that of the H18 atom since nitrogen atoms attract a lot of electrons. However, it may not be easily attacked by the nucleophile since H18, with the maxima in a monomer, and N, with surface minima in neighboring monomer product hydrogen bond, will result in the electrostatic potentials cancelling each other out. The same applies to H17, with the other global maxima site at $+52.62 \text{ kcal mol}^{-1}$. From Figure 7(b), it can be seen that a large portion has a small ESP value from -25 to $+25 \text{ kcal mol}^{-1}$. The negative part mainly corresponds to the surface above and below the several N atoms with the effect of the abundant lone-pair electron or π -electron cloud. The largest positive area mainly arises from the C-C double bond, and the smaller ones with remarkable positive ESP values correspond to the C-H bond, though these are not nucleophilic sites.

The electrostatic potential map of the molecular surface (a) and the surface areas in each ESP range (b) of N18 is plotted and shown in Figure 8. The surface minima of ESP are distributed in the peripheral of the N-atom ring and their values range from -17.15 to $-17.16 \text{ kcal mol}^{-1}$, which is close to global minima. The N25 is near the global minima site, with the value $-17.16 \text{ kcal mol}^{-1}$. Just like the minima, the surface maxima ranges from $+42.00$ to $+42.14 \text{ kcal mol}^{-1}$, which is close to the global maxima $+42.17 \text{ kcal mol}^{-1}$. They are located on the periphery of the benzene ring and on the same side as the global minima site. It can be seen that positive and negative potentials are distributed more evenly over the surface. There is a large portion ESP distributing from -20 to $+30 \text{ kcal mol}^{-1}$, as shown in Figure 8(b). Obviously, the positive part arises from the N atom and the negative one comes from the C atom.

Heats of formation

The gas phase heat of formation of N14 and N18 can be calculated according to Figure 2, 3 and Equation (1). The experimental gas phase heat of formation of NH_3 , CH_4 , C_6H_6 , CH_3NH_2 , N_2H_2 , and N_2H_4 are available.²⁷ They are all shown in Table 4 and the gas phase heat of formation of N14 and N18 are 2142.17 and $2959.60 \text{ kJ mol}^{-1}$, respectively. Due to the great deal of nitrogen atoms that are connected directly, their enthalpy of formation is much higher than RDX, HMX, or CL-20,¹⁸ as shown in Table 7.

The heat of formation in the condensed phase of N14 and N18 can be calculated according to Equations (2) and (3), and they are 2048.49 and $2846.46 \text{ kJ mol}^{-1}$, respectively. Related parameters are shown in Table 5.

Crystal densities

The crystal densities of N14 and N18 can be calculated according to Equation (4), and they are 1.784 and 1.817 g cm^{-3} . Related parameters are shown in Table 6. As these two compounds contain mainly C and N, and do not contain O, and their densities are lower than HMX and CL-20, as shown in Table 7. The density of nitrogen-rich compounds without oxygen atoms is generally low. For instance, the density value of hydrogen azide (HN_3) and 5-amino-1H-tetrazole is 1.12 and 1.71 g cm^{-3} respectively.²⁷ When it comes to

Table 3. Energy gaps of some compounds

Comp	B3LYP			ω B97X-D		
	LUMO(au)	HOMO(au)	ΔE (au)	LUMO(au)	HOMO(au)	ΔE (au)
N14	-0.10351	-0.25456	0.15105	-0.02412	-0.32465	0.30053
N18	-0.12522	-0.27532	0.15010	-0.05100	-0.34487	0.29387

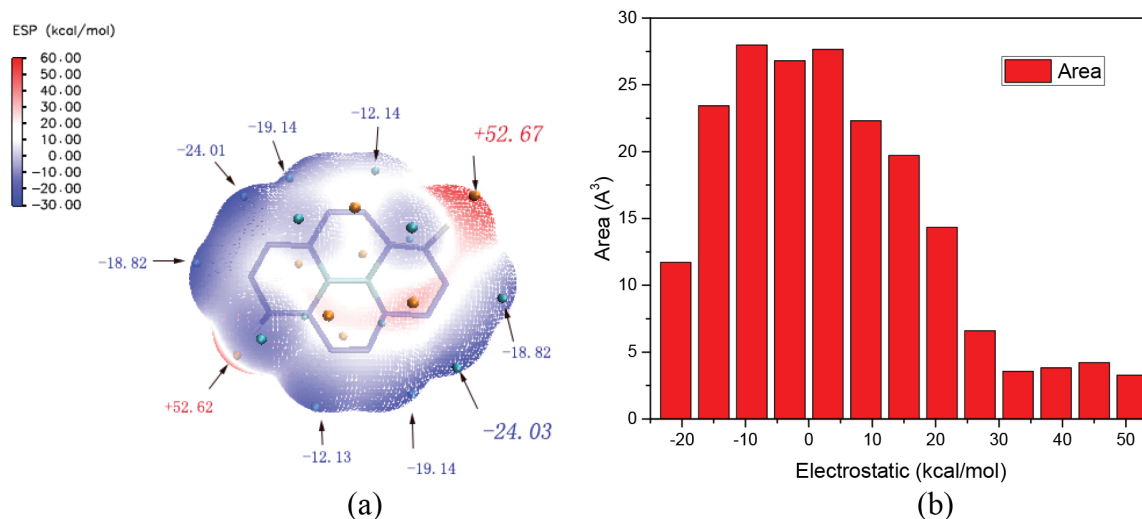


Figure 7. Electrostatic potentials map (a) and the surface areas (b) of N14

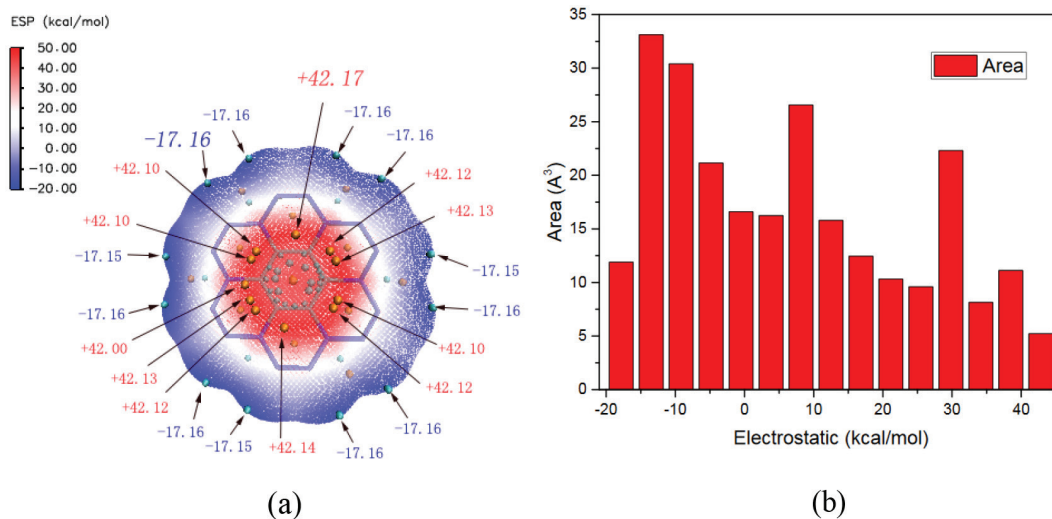


Figure 8. Electrostatic potentials map (a) and the surface area (b) of N18

Table 4. Related parameters for predicting gas phase heat of formation by isodesmic reactions

Comp	$E_{\text{ZPE}}(\text{au})$	$H_{\text{T}}(\text{au})$	$E_0(\text{au})$	$\Delta H_{\text{f}}(\text{g})$ (kJ mol ⁻¹)
N18	0.119786	0.016010	-1213.869725	2959.60
N14	0.101568	0.011946	-843.6855212	2142.17
CH ₄	0.044539	0.003813	-40.53396275	-74.60
NH ₃	0.034252	0.003818	-56.58272201	-45.90
C ₆ H ₆	0.100085	0.005347	-232.3113072	82.90
C ₂ H ₄	0.050775	0.003986	-78.61553852	52.40
CH ₃ NH ₂	0.063782	0.004380	-95.89388879	23.50
N ₂ H ₂	0.027332	0.003801	-110.6779937	197.07
N ₂ H ₄	0.053284	0.004203	-111.9106874	95.35

Table 5. Related parameters for predicting condensed phase heat of formation

Comp	A_{s} (Å ²)	σ_{tot}^2 ([kcal mol ⁻¹]²)	v	H_{sub} (kJ mol ⁻¹)	$\Delta H_{\text{f}}(\text{c})$ (kJ mol ⁻¹)
N18	250.95424	170.1758509	0.11375910	113.14	2846.46
N14	195.50755	206.0047982	0.15147528	93.68	2048.49

traditional CHON materials, their heats derive from redox reaction and the density is an important parameter to power.²⁸ But compounds mentioned in title are more like polynitrogen compounds, their heats derive from the deviation of bond energy of each nitrogen atom.⁸ Therefore, the density is not the primary focus.

Detonation performance

The detonation velocity (D), detonation pressure (P), and heat of detonation (Q) of N14 and N18 are computed based on their crystal densities (ρ) and condensed phase heats of formation $\Delta_{\text{f}}H(\text{c})$. Their detonation performance, including RDX, HMX, and CL-20,²⁹ are shown in Table 7. It is surprised that crystal density and heat of formation of N14 is lower than that of N18, but the detonation performance of the former is greater than that of the latter. Because the number mole of gaseous detonation products per gram of explosive

Table 6. Related parameters for predicting crystal densities

Comp	V_m ($\text{cm}^3 \text{mol}^{-1}$)	M (g mol^{-1})	$v\sigma^2$ ($[\text{kcal mol}^{-1}]^2$)	ρ_{cry} (g cm^{-3})
N18	173.12408	324	19.3590517	1.82
N14	122.81914	221	31.2046336	1.78

plays a key role in detonation performance here. This result also reveals that detonation performance of N14 ($Q = 2214 \text{ cal g}^{-1}$ and $D = 10,040 \text{ m s}^{-1}$) and N18 ($Q = 2114 \text{ cal g}^{-1}$ and $D = 9400 \text{ m s}^{-1}$) are higher than that of CL-20, while their detonation pressures (43.6 GPa and 37.4 GPa) are lower. The title compounds can decompose into large amount of nitrogen gas, which contributes to their detonation performance. Nitrogen-rich molecules are thus designed to promising materials. For example, dinitropyrazole fused 1,2,3,4-tetrazine has a performance ($D=9631 \text{ m s}^{-1}$, $P=44.0 \text{ GPa}$) comparable to CL-20.³⁰

Table 7. Performance parameters of HEDMs

Comp	ρ (g cm^{-3})	$\Delta_f H(c)$ (kJ mol^{-1})	Q (cal g^{-1})	D (m s^{-1})	P (GPa)
N18	1.82	2846.46	2114	9400	37.4
N14	1.78	2048.49	2214	10,040	43.6
RDX ^a	1.80	79.00	1501	8750	34.7
HMX ^a	1.90	102.41	1498	9100	39.3
ϵ -CL-20 ^a	2.04	377.04	1567	9380	44.1

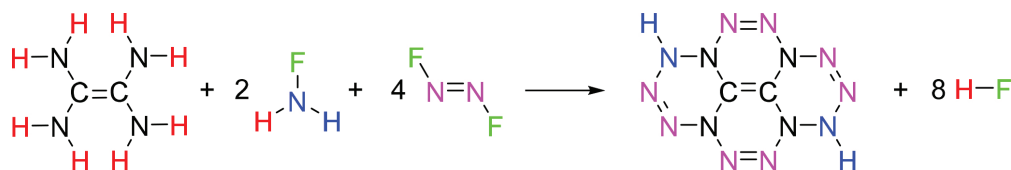
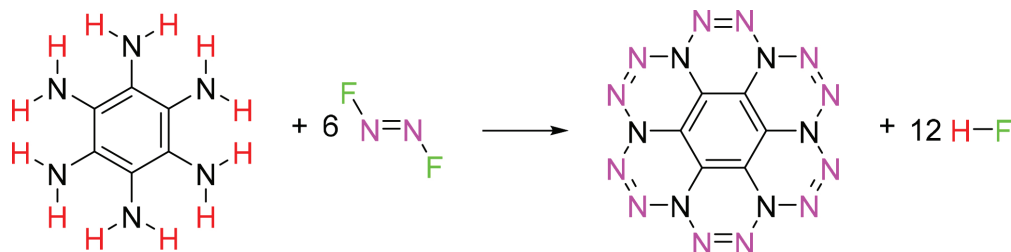
^aThe detonation performance values are from reference.²⁹

Impact sensitivity

The values (cm) of $h_{50\%}$ are estimated through the method and the results are summarized in Table 8. The calculated sensitivity of CL-20 is 9 cm, closing to measured value.¹⁶ The values of title compounds are 23 and 32 cm respectively, and higher than CL-20. Therefore, the N14 and N18 are more insensitivity than CL-20. Compounds in which many nitrogen atoms are directly connected are all sensitive to impact, and a common example is lead azide.³¹ But when these nitrogen atoms constitute a fused ring, the sensitivity will be improved.^{30,32}

SYNTHETIC ROUTES

It is well known^{33,34} that the N-F bond is weak to break, and

**Figure 9.** A possible route to prepare N14**Figure 10.** A possible route to prepare N18**Table 8.** Impact sensitivities of title compounds and CL-20

Comp	σ_s^2 ($[\text{kcal mol}^{-1}]^2$)	v	h_{cal} (cm)	h_{exp} (cm)
CL-20	246.03124	0.05923738	9	14 ^a
N18	147.90124	0.1137591	23	-
N14	167.66452	0.15147528	32	-

^aThe value is from reference.¹⁶

then hydrogen fluoride is eliminated. Based on that, polynitrogen material N_5^+ was synthesized.⁸ The same method is also used to produce the title compounds and two possible routes were proposed in Figure 9 and 10. In the two schemes, tetraaminoethylenes,³⁵ hexaaminobenzene,³⁶ monofluoroamin,³⁷ and 1,2-difluorodiazine³⁸ are obtained in accordance with previous papers.

CONCLUSIONS

In this work, N14 and N18 are calculated by the Gaussian 09 package with the B3LYP method with the 6-311++G (d, p) basis set to investigate their detonation performance and stability. The results show that the detonation performance of N14 ($P = 43.6 \text{ GPa}$, $D = 10,040 \text{ m s}^{-1}$, $Q = 2214 \text{ cal g}^{-1}$) and N18 ($P = 37.4 \text{ GPa}$, $D = 9400 \text{ m s}^{-1}$, $Q = 2114 \text{ cal g}^{-1}$) are comparable to the value of CL-20. All the atoms in the two compounds may form a special conjugated system although they are non-coplanar, and this requires further discussion. Considering both the detonation properties and relative stabilities, they are all likely to be used as candidates of high energy density materials with modest impact sensitivity and high performance, and these results can also be used for comparisons with properties of other familiar explosives, and provide theoretical support for the molecular design of novel high energetic density compounds. Further work on route optimization and practical synthesis is being carried out by our team.

SUPPLEMENTARY MATERIAL

Tables 1S – 4S can be freely accessed at <http://www.quimicanova.s bq.org.br>, in PDF format.

ACKNOWLEDGEMENTS

This work was supported by the National Natural Science Foundation of China (NO.21576026).

REFERENCES

1. Dong, Y.; Peng, P.; Hu, B.; Su, H.; Li, S.; Pang, S.; *Molecules* **2017**, *22*.
2. Lv, P.; Tong, Y.; Wang, H.; Dang, L.; Sun, C.; Pang, S.; *J. Mol. Liq.* **2017**, *231*, 192.
3. Chen, J.; Yu, Y.; Li, Y.; Pang, S.; *J. Fluorine Chem.* **2018**, *205*, 35.
4. Zhang, Q.; Shreeve, J. M.; *Angew. Chem., Int. Ed. Engl.* **2013**, *52*, 8792.
5. Xu, Y.; Wang, Q.; Shen, C.; Lin, Q.; Wang, P.; Lu, M.; *Nature* **2017**, *549*, 78.
6. Meng, L.; Lu, Z.; Wei, X.; Xue, X.; Ma, Y.; Zeng, Q.; Fan, G.; Nie, F.; Zhang, C.; *CrystEngComm* **2016**, *18*, 2258.
7. Christe, K. O.; *Propellants, Explos., Pyrotech.* **2007**, *32*, 194.
8. Christe, K. O.; Wilson, W. W.; Sheehy, J. A.; Boatz, J. A.; *Angew. Chem., Int. Ed.* **2001**, *40*, 2947.
9. Eremets, M. I.; Gavriluk, A. G.; Trojan, I. A.; Dzivenko, D. A.; Boehler, R.; *Nat. Mater.* **2004**, *3*, 558.
10. Zhang, C.; Sun, C.; Hu, B.; Yu, C.; Lu, M.; *Science* **2017**, *355*, 374.
11. Zhang, W.; Wang, K.; Li, J.; Lin, Z.; Song, S.; Huang, S.; Liu, Y.; Nie, F.; Zhang, Q.; *Angew. Chem., Int. Ed. Engl.* **2018**, *57*, 2592.
12. Strout, D. L.; *J. Phys. Chem. A* **2002**, *106*, 816.
13. Mondal, S.; Srinivasu, K.; Ghosh, S. K.; Chattaraj, P. K.; *RSC Adv.* **2013**, *3*, 6991.
14. Tawar, T.; Kerim, A.; *Fullerenes, Nanotubes, Carbon Nanostruct.* **2015**, *23*, 846.
15. Frisch, M. J.; Trucks, G. W.; Schlegel, H. B.; Scuseria, G. E.; Robb, M. A.; Cheeseman, J. R.; Scalmani, G.; Barone, V.; Petersson, G. A.; Nakatsuji, H.; Li, X.; Caricato, M.; Marenich, A. V.; Bloino, J.; Janesko, B. G.; Gomperts, R.; Mennucci, B.; Hratchian, H. P.; Ortiz, J. V.; Izmaylov, A. F.; Sonnenberg, J. L.; Williams-Young, D.; Ding, F.; Lipparini, F.; Egidi, F.; Goings, J.; Peng, B.; Petrone, A.; Henderson, T.; Ranasinghe, D.; Zakrzewski, V. G.; Gao, J.; Rega, N.; Zheng, G.; Liang, W.; Hada, M.; Ehara, M.; Toyota, K.; Fukuda, R.; Hasegawa, J.; Ishida, M.; Nakajima, T.; Honda, Y.; Kitao, O.; Nakai, H.; Vreven, T.; Throssell, K.; Montgomery, J. A., Jr.; Peralta, J. E.; Ogliaro, F.; Bearpark, M. J.; Heyd, J. J.; Brothers, E. N.; Kudin, K. N.; Staroverov, V. N.; Keith, T. A.; Kobayashi, R.; Normand, J.; Raghavachari, K.; Rendell, A. P.; Burant, J. C.; Iyengar, S. S.; Tomasi, J.; Cossi, M.; Millam, J. M.; Klene, M.; Adamo, C.; Cammi, R.; Ochterski, J. W.; Martin, R. L.; Morokuma, K.; Farkas, O.; Foresman, J. B.; Fox, D. J.; *Gaussian 09 Revision A.1.*, Gaussian Inc, 2009.
16. He, P.; Zhang, J. G.; Wang, K.; Yin, X.; Zhang, T. L.; *J. Org. Chem.* **2015**, *80*, 5643.
17. He, P.; Zhang, J. G.; Wu, L.; Wu, J. T.; Zhang, T. L.; *J. Phys. Org. Chem.* **2017**, *30*, 3674.
18. Qi, C.; Li, S. H.; Li, Y. C.; Wang, Y.; Zhao, X. X.; Pang, S. P.; *Chem. - Eur. J.* **2012**, *18*, 16562.
19. Lin, H.; Zhu, Q.; Huang, C.; Yang, D.; Lou, N.; Zhu, S.; Li, H.; *Struct. Chem.* **2019**.
20. Jin, X.; Zhou, J.; Wang, S.; Hu, B.; *Quim. Nova* **2016**, *39*, 467.
21. Humphrey, W.; Dalke, A.; Schulten, K.; *J. Mol. Graphics* **1996**, *14*, 33.
22. Lu, T.; Chen, F.; *J. Comput. Chem.* **2012**, *33*, 580.
23. Byrd, E. F. C.; Rice, B. M.; *J. Phys. Chem. A* **2006**, *110*, 1005.
24. Politzer, P.; Martinez, J.; Murray, J. S.; Concha, M. C.; Toro-Labbé, A.; *Mol. Phys.* **2009**, *107*, 2095.
25. Tsai, C.; Su, Y.; Li, G.; Chai, J.; *Phys. Chem. Chem. Phys.* **2013**, *15*, 8352.
26. Pospisil, M.; Vavra, P.; Concha, M. C.; Murray, J. S.; Politzer, P.; *J. Mol. Model.* **2010**, *16*, 895.
27. <https://webbook.nist.gov/chemistry/>, accessed in August 2019.
28. Kamlet, M. J.; Jacobs, S. J.; *J. Chem. Phys.* **1967**, *48*, 1.
29. Politzer, P.; Murray, J. S.; *Cent. Eur. J. Energ. Mater.* **2011**, *8*, 209.
30. Tang, Y.; Kumar, D.; Shreeve, J. M.; *J. Am. Chem. Soc.* **2017**, *139*, 13684.
31. Deng, M.; Feng, Y.; Zhang, W.; Qi, X.; Zhang, Q.; *Nat. Commun.* **2019**, *10*, 1339.
32. Li, Y. C.; Qi, C.; Li, S. H.; Zhang, H. J.; Sun, C. H.; Yu, Y. Z.; Pang, S. P.; *J. Am. Chem. Soc.* **2010**, *132*, 12172.
33. Belter, R. K.; *J. Fluorine Chem.* **2011**, *132*, 961.
34. Peng, W.; Shreeve, J. M.; *J. Org. Chem.* **2005**, *70*, 5760.
35. Winberg, H. E.; Carnahan, J. E.; Coffman, D. D.; Brown, M.; *J. Am. Chem. Soc.* **1965**, *87*, 2055.
36. Lahiri, N.; Lotfizadeh, N.; Tsuchikawa, R.; Deshpande, V. V.; Louie, J.; *J. Am. Chem. Soc.* **2017**, *139*, 19.
37. Minkwitz, R.; Nass, R.; *ChemInform* **1989**, 20.
38. Sanborn, R. H.; *J. Chem. Phys.* **1960**, *33*, 1855.